

Laboratory Observations of the Zeeman Effect

Jack Nelson,
Physics Department,
Occidental College, Los Angeles, CA

November 2016

Abstract

1 Introduction

1.1 Historical Background

1.2 Theoretical Overview

The splitting of the spectra of mercury into hyperfine lines when an external magnetic field is applied is the result of the mercury atom's magnetic-dipole interaction with the external magnetic field.

In its ground state, the mercury atom has 80 electrons in which the $n = 1, 2, 3, 4$, and 5 shells are filled, leaving two $6s$ valence electrons. The spectral emissions of mercury come from the transitions of these two valence electrons between different quantum states. Figure 4 shows the different possible transitions of the mercury atom. Our observations will be limited to the $7^3S_1 \rightarrow 6^3P_2$ transition which yields the 546.1 nm green spectral line.

When no external magnetic field is present, hyperfine structure in atomic spectra can be observed due to the spin-angular momentum coupling of electrons. See pp. 47 of [2] for a more detailed discussion. In the presence of an external magnetic field, the interaction of the total angular momentum of the electrons with the magnetic field also splits the spectral lines into finer lines of slightly different wavelength. Figure 1 shows how a single transition from the $l = 2$ to $l = 1$ states results in hyperfine structure in the presence of a magnetic field.

The following discussion is a summary of that in chapter 2 of [2] on the Zeeman Effect. For a more de-

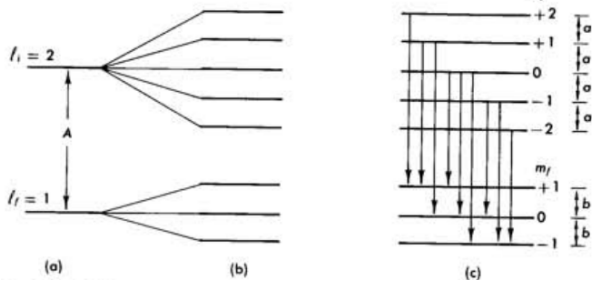


Figure 1: A single spectral line caused by an atomic energy transition will be split into multiple “hyperfine” lines due to the interaction of the total angular momentum of the valence electrons with an external magnetic field. (a) shows the transition in the absence of an external magnetic field. The transition between the $l = 2$ and the $l = 1$ states ($d \rightarrow p$) produces a single spectral line. (b) shows how these formerly single energy-levels are split into multiple states in the presence of an external magnetic field. (c) shows the possible transitions between the new states, each of which produces a different spectral line with slightly different wavelength.

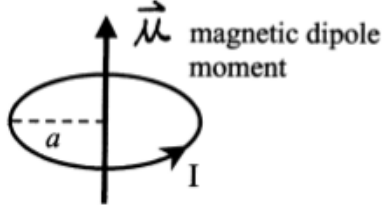


Figure 2: A loop of current about a vertical axis with magnetic moment μ .

tained discussion of the derivation and consequences, consult that reference.

Hyperfine splitting in the presence of a magnetic field is due to the interactions of the valence electrons with the magnetic field. These interactions result in an added energy ΔE per electron given by

$$\Delta E = m\mu_0 H \quad (1)$$

where m is the mass of the electron, μ_0 is the Bohr Magneton, fundamental magnetic moment of the electron, and H is the applied magnetic field.

To understand the origin of these interactions, consider a simple current loop such as the one shown in Figure 2. The associated magnetic moment μ of the loop has the magnitude:

$$\mu = IA \quad (2)$$

Where $A = \pi a^2$ is the disk area enclosed by the loop. The direction of μ is given by the right-hand rule.

When an external magnetic field \mathbf{B} is applied, the torque on the loop is given by

$$\tau = \mu \times \mathbf{B} \quad (3)$$

The resulting potential energy of the current loop in the magnetic field is

$$E_B = -\mu \cdot \mathbf{B} \quad (4)$$

That is, the magnetic field will do work on the current loop when its orientation is changed in the field.

The Bohr Magneton arises from modeling the electron classically as a current loop with current density

$$\mathbf{J}(\mathbf{x}) = -ev\delta(\mathbf{x} - \mathbf{r}) \quad (5)$$

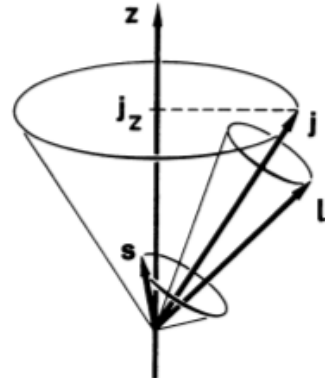


Figure 3: Electron spin angular momentum \mathbf{s} and orbital angular momentum \mathbf{l} sum to create total angular momentum \mathbf{j} .

Where \mathbf{r} is the orbit equation and \mathbf{x} is the electron position.

This current density results in a magnetic dipole moment given by

$$\mathbf{u} = \frac{1}{2c} \int \mathbf{x} \times \mathbf{J}(\mathbf{x}) d^3x = -\frac{1}{2c} e(\mathbf{r} \times \mathbf{v}) \quad (6)$$

The angular momentum of the orbit is given by

$$\mathbf{L} = \mathbf{r} \times \mathbf{p} = m_e (\mathbf{r} \times \mathbf{v}) \quad (7)$$

The quantized angular momentum of the electron is given by

$$\mathbf{L} = \frac{lh}{2\pi} \quad (8)$$

The total angular momentum j of mercury is dependent on both the orbital angular momentum of the valence electrons given by the quantum number l , and the spin angular momentum quantum number s . In Russell-Saunders or LS coupling, the total angular momentum is given by the sum of the orbital angular momentum and the spin angular momentum:

$$j = l + s \quad (9)$$

Figure 3 shows how these two quantities (vectors, actually) combine to form total angular momentum.

Selection rules place restrictions on how the quantum numbers may change when a valence electron undergoes a transitions. These selection rules are:

1. $\Delta s = 0$
2. $\Delta l = 0, \pm 1$
3. $\Delta J = 0, \pm 1$, but not $\Delta J = 0 \rightarrow \Delta J = 0$
4. $\Delta M_j = 0, \pm 1$, but not $M_j = 0 \rightarrow M_j = 0$ if $\Delta J = 0$

Figure 1 shows that spectral splitting is dependent on the magnetic quantum number m which specifies the projection of the orbital angular momentum along the z-axis of the atom. m can take on $2l + 1$ the values ranging from l to $-l$.

The polarization of the emitted light during the transition is also entirely determined by Δm_j . For $\Delta m_j = 0$, the emitted photons are polarized linearly and parallel to the field lines of the applied magnetic field \mathbf{B} . For $\Delta m_j = \pm 1$, emitted photons are circularly polarized along the direction of \mathbf{B} and appear linearly polarized perpendicular to \mathbf{B} when viewed side-on to \mathbf{B} .

The energy difference between the hyperfine spectra is caused by the differing values of Δm and determined by measuring the relative differences in wavelength between the fine spectra. From the basic Planck relation we have

$$E = h\nu = \frac{hc}{\lambda} \quad (10)$$

where h is the Planck constant, ν is wave frequency, and λ is wavelength.

The relative energy difference of two wavelengths is then given by

$$\Delta E = - \left(\frac{hc}{\lambda^2} \right) \Delta \lambda \quad (11)$$

$$g_L = 1 + \frac{J(J+1) + S(S+1) - L(L+1)}{2J(J+1)} \quad (12)$$

$$\Delta E = M_z g_L B \mu_B \quad (13)$$

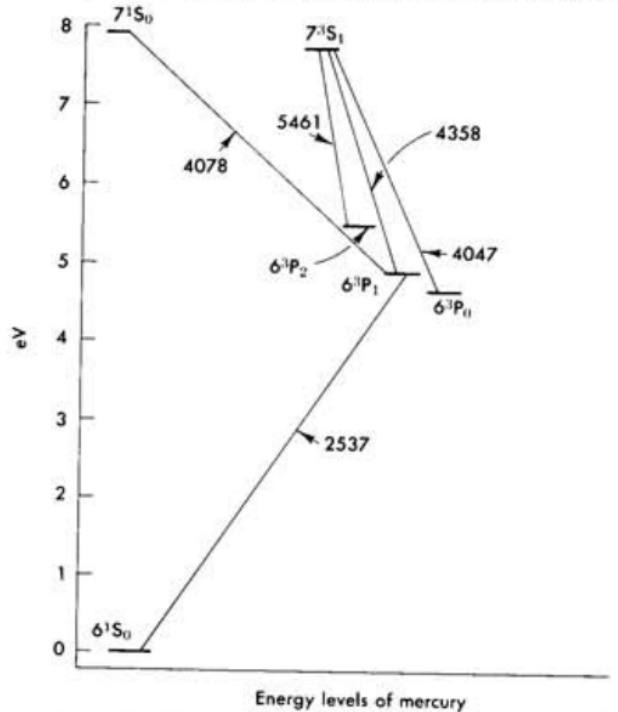


Figure 4: Energy level transitions of mercury between quantum states. For the purposes of our observations, we are interested in the $7^3S_1 \rightarrow 6^3P_2$ transition which produces 546.1 nm light. Figure 7.39 of [2]

1.3 Calculation of the Bohr Magneton

The fundamental unit of magnetic moment, the Bohr magneton, is given by

$$\mu_B = \frac{eh}{4\pi m_e} \quad (14)$$

where m_e is the electron mass, e is the electron charge, and h is Planck's constant. We are interested in measuring this fundamental quantity through observation. To do so, we will measure the magnitude of the hyperfine spectral line splitting in the presence of a magnetic field, and relate this splitting to the magnitude of the Bohr magneton.

Consider the 546.1 nm mercury line in the presence of a magnetic field. As described in the previous section, the interaction of the spin-coupled total angular momentum of the valence electrons will interact with the magnetic field to produce hyperfine structure with energy, and thus wavelength, dependent on the value of ΔM_z in the transition.

For the case of $M_z = 0 \rightarrow M_z = 0$, the resulting spectral line will be the same as the un-split spectral line in the $B = 0$ case with $\lambda = 546.1\text{nm}$. In the $M_z = +1 \rightarrow M_z = +1$ and $M_z = -1 \rightarrow M_z = -1$ cases, however, the resulting hyperfine spectral line will be of slightly greater or less energy than the $B = 0$ spectral line, thus resulting in a "triplet" hyperfine structure in which the central 546.1 nm spectral line is surrounded on either side by two additional hyperfine spectral lines.

We calculate the Landé g-factor for both the S and P states using equation (12). For the 3S_1 state, $L = 0$ and $S = 1$, thus $J = 1$, and $g_S = 2$. For the 3P_2 state, $L = 1$ and $S = 1$, thus $J = 2$, and $g_P = 3/2$.

Thus, using equation (13), the energy shifts for the $M_z = \pm 1$ cases for the S and P states in the presence of a magnetic field will be:

$$\Delta E_S = \pm 2B\mu_B \quad (15)$$

$$\Delta E_P = \pm \frac{3}{2}B\mu_B \quad (16)$$

Thus, the photon energy for the $M_z = +1 \rightarrow M_z = +1$ transition will be

$$E = h\nu_+ = (E_S + \Delta E_S) - (E_P + \Delta E_P) \quad (17)$$

and for the $M_z = -1 \rightarrow M_z = -1$ it will be

$$E = h\nu_- = (E_S - \Delta E_S) - (E_P - \Delta E_P) \quad (18)$$

The difference in energy between the two hyperfine lines will then be

$$h(\nu_+ - \nu_-) = 2(\Delta E_S - \Delta E_P) \quad (19)$$

Which is then related to the Bohr magneton by

$$2(\Delta E_S - \Delta E_P) = 2 \left(2B\mu_B - \frac{3}{2}B\mu_B \right) = B\mu_B \quad (20)$$

Thus we have a relation for the difference between the inner and outer hyperfine spectra frequencies (and therefore their wavelengths), and the value of the Bohr magneton.

$$h(\nu_+ - \nu_-) = B\mu_B \quad (21)$$

We convert these frequencies to wavelengths using the fundamental relation $f = c/\lambda$

$$h \left(\frac{c}{\lambda_+} - \frac{c}{\lambda_-} \right) = \frac{hc(\lambda_- - \lambda_+)}{\lambda_- \lambda_+} \quad (22)$$

$$= \frac{hc\Delta\lambda}{\lambda^2} = B\mu_B \quad (23)$$

where $\lambda_- \lambda_+ = \lambda^2$ to a good approximation because of the very small difference in wavelength between the hyperfine spectra.

Rearranging, we have

$$\Delta\lambda = \frac{B\mu_B\lambda^2}{hc} \quad (24)$$

We now have a relation between the change in wavelength between the outer hyperfine spectra and the Bohr magneton. We must now develop a method and theory of measuring these very slight differences in wavelength. This is accomplished using a Fabry-Perot interferometer to make these slight wavelength differences measurable.

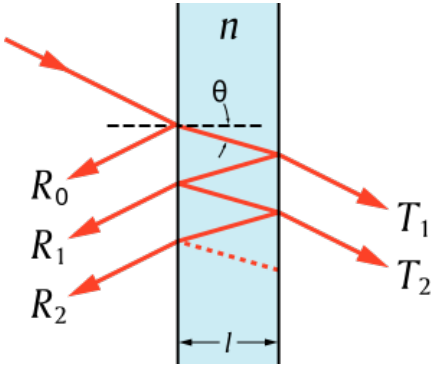


Figure 5: Cross-section of the Fabry-Perot etalon. Light entering the etalon undergoes multiple internal reflections before being reflected or transmitted externally. In our notation, the etalon gap distance l is referred to as d .[3]

1.3.1 Fabry-Perot Interferometer

In order to measure very slight wavelength differences, we employed a Fabry-Perot interferometer. The main mechanism of the interferometer is the etalon, which consists of two partially optically reflected glass plates very precisely aligned parallel to each other.

$$\frac{d}{f^2} \lambda = \frac{k}{(R_k^2 - R_0^2)} = C_0 \quad (25)$$

Where d is the gap distance of the Fabry-Perot etalon, approximately 1.995 mm.

$$\mu_B = \left(\frac{C_0 hc}{2dB} \right) (R_{k+}^2 - R_{k-}^2) \quad (26)$$

2 Methods and Procedures

The Pasco Scientific Model SE-9654 Zeeman Effect Experiment was used to make all observations. The experiment consisted of two large solenoids oriented along the same axis with an air gap between them in which a mercury lamp was placed. An optical rail was used to align a polarizing filter, a collimating lens, an interference filter, a Fabry-Perot interferometer, and a CMOS camera. The basic experimental

technique consisted of imaging the interference pattern of the 546.1 nm mercury spectral line with the CMOS camera through the polarizer and Fabry-Perot interferometer. Figure

To study the Zeeman effect, observations of a mercury lamp were made first with no magnetic field and 90 deg polarization, then with an approximately 1T magnetic field. Observations with a magnetic field included:

- 90 deg (field-perpendicular) polarization
- 0 deg (field-parallel) polarization
- No polarization
- Axial B-field at polarization varying from 90 deg to 0 deg

Figure 8 shows the perpendicular and axial configurations of the magnetic field used for the observations.

The observations and results of each of these field configurations will be presented and discussed in Section 3.

2.1 Method Description

3 Data and Results

With no applied magnetic field, the 546.1nm mercury spectral line as viewed through the Fabry-Perot interferometer produces the interference pattern as shown in Figure 9. The $B = 0$ interference pattern shows discrete rings, with the innermost ring denoted as the $k = 0$ ring, the next innermost ring the $k = 1$ ring, and so on.

Table 1 shows the measured radii of the interference rings for the $k = 1$ through $k = 4$ rings. The $k = 0$ ring was not used in subsequent observations and calculations because it was not resolved enough to be measurable.

The “bullseye” $B = 0$ pattern will be the standard interference pattern we will compare all subsequent patterns on.

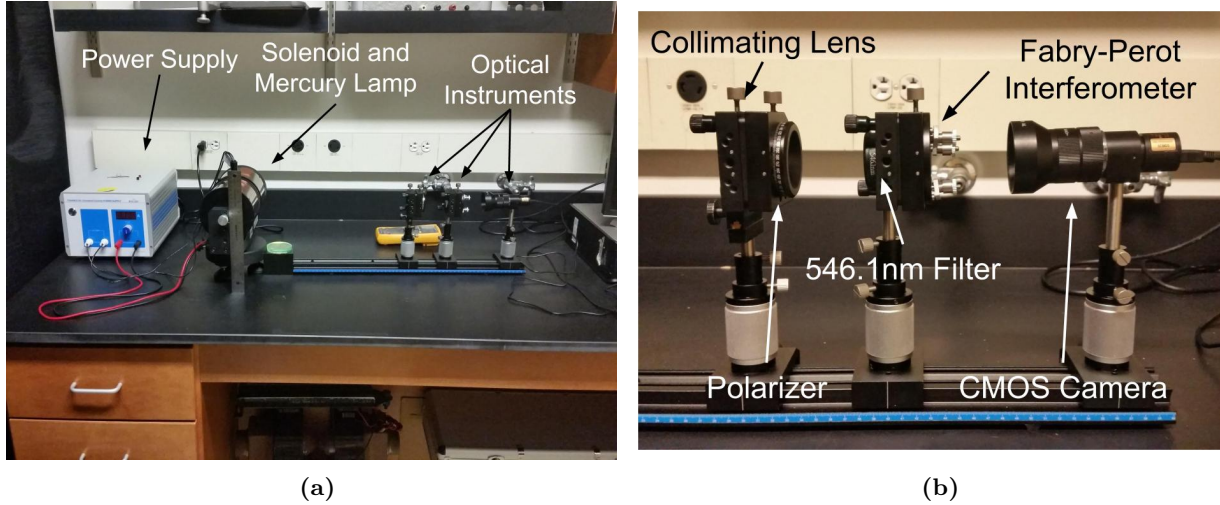


Figure 6: Overview of the Experiment configuration. Figure 6a shows the entire apparatus with the variable power supply for the solenoid and mercury lamp, the solenoid, the mercury lamp (hidden by the solenoid), the optical track, and the optical instruments. Figure 6b shows the optical instruments in detail.

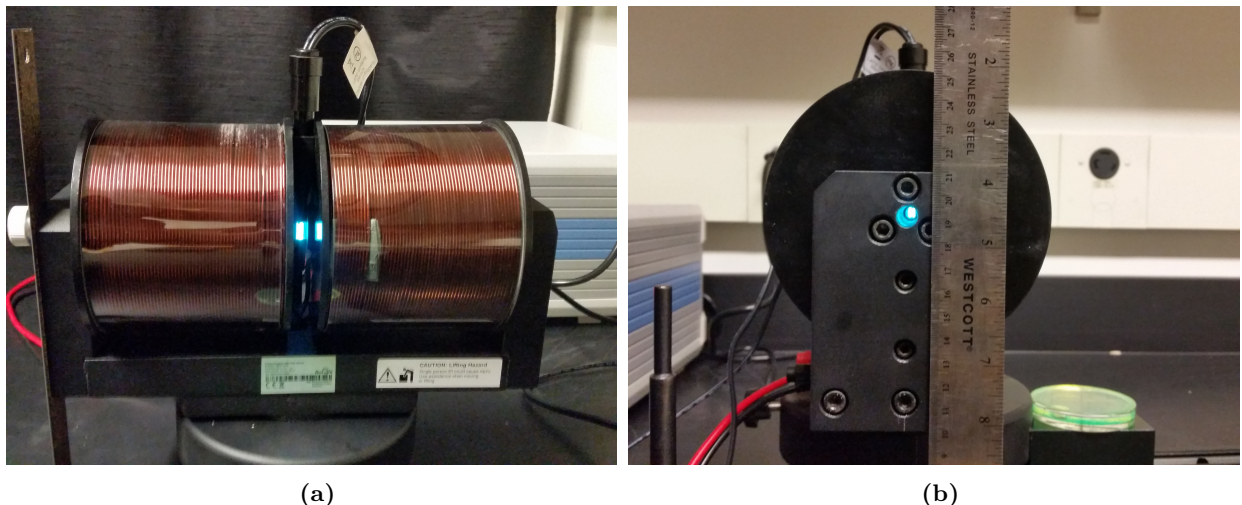


Figure 7: Detail view of the solenoid with the mercury lamp source. Figure 7a shows the configuration with the magnetic field lines perpendicular to the light source. Figure 7b shows the axial field configuration looking down the sight-hole of the solenoid to the mercury lamp.

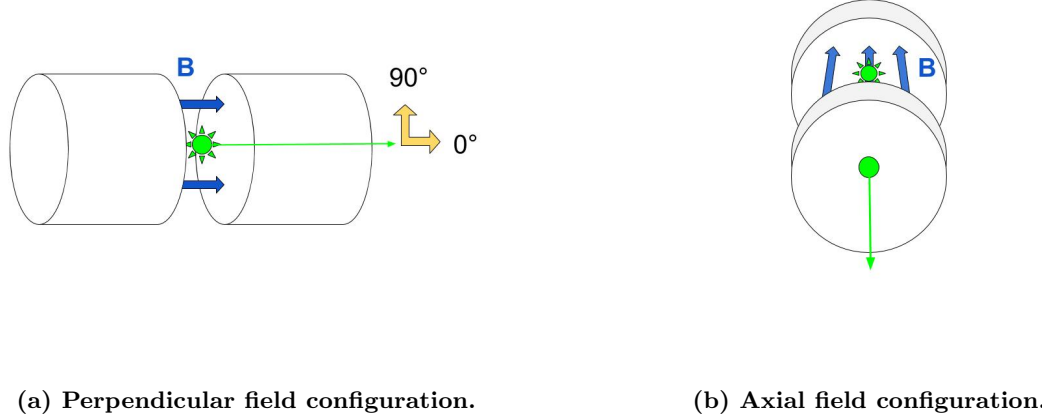


Figure 8: The two magnetic field configurations observed. In (8a), the magnetic field is oriented perpendicularly to the path of the observed light from the mercury lamp. 90° polarization is defined to be perpendicular to the field lines, while 0° polarization is parallel to the field lines. In configuration (8b), light from the lamp travels along the magnetic field lines down the center of one of the solenoids through a sight hole.

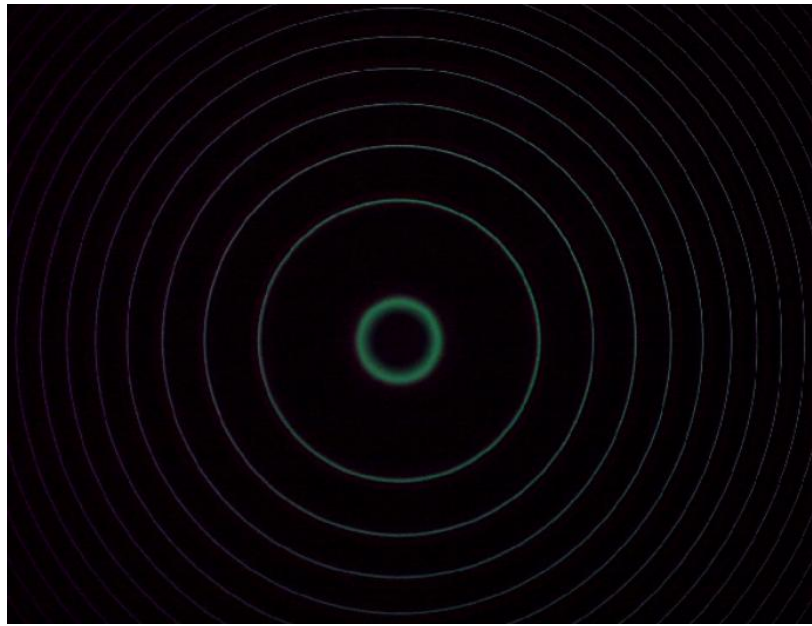


Figure 9: Interference pattern of the 546.1nm mercury line with no applied magnetic field. The interference lines are singular.

k	Radius (m)
4	$0.7956 \pm 0.1 \times 10^{-3}$
3	$0.6911 \pm 0.2 \times 10^{-3}$
2	$0.5678 \pm 0.1 \times 10^{-3}$
1	$0.4096 \pm 0.1 \times 10^{-3}$

Table 1: Interference ring radii of the mercury 546.1 nm spectra with no magnetic field.

3.1 Observations perpendicular to the Magnetic Field

The first observations were made such that the mercury lamp was viewed perpendicularly to the magnetic field, as is shown in Figure 8a.

When viewed without a polarizer, the interference pattern appears as in Figure 10. All nine of the transition spectra, corresponding to all 9 possible ΔM_z transition values, can be seen.

From the theory discussed in section 1.2, different values of ΔM_z in the mercury transition will produce different polarizations of the emitted light. Thus, we can use polarization to identify particular hyperfine lines which correspond to certain values of ΔM_z .

3.1.1 $\Delta M_z = 0$ Transition spectra

With a 1T magnetic field and the polarizer set parallel to the field lines, we observed the mercury spectra with polarization parallel to the applied magnetic field. A distinct triple ring structure can be seen Figure 11 in which each interference ring consists of a bright central ring surrounded by two fainter rings. This is what has been historically termed the “Normal” Zeeman effect.

Using PASCO Software, The radii of the inner and outer rings of the $k = 1$ through $k = 4$ interference rings were measured. These radii are given in Table 2 and will be used to calculate the value of the Bohr magneton in Section 3.3.

3.1.2 $\Delta M_z = \pm 1$ Transition Spectra

3.2 Spectra Along an Axial Magnetic Field

3.3 Measurement of the Bohr Magneton

Using the measurements of the split interference rings from the $B \neq 0$ case we were able to establish a value for the Bohr magneton. The inner and outer radius of each interference triplet was measured using PASCO software and is tabulated in Table 2.

To calculate the magnitude of the Bohr magneton, we use the theory from Section 1.3. First, we must calculate the constant C_0 in equation (25). This is accomplished using the un-split interference ring radii from the $B = 0$ case. These measurements are given in Table 1.

Using equation (25), the value of C_0 for each interference ring $k = 1$ through $k = 4$ was calculated. The average of these values was then taken as the best value for C_0 . Table 3 lists the calculated values for each interference ring, as well as the overall mean and standard deviation.

With a precise measured value for C_0 , values for the Bohr magneton can then be calculated with equation (26). The difference between inner and outer radii for each interference ring in the $B \neq 0$, parallel-field polarization case, which is related to the magnitude of the change in wavelength between the $\delta M_z = \pm 1$ transitions, is used to calculate the Bohr magneton. These values for R_{k+} and R_{k-} are given in Table 2.

The remaining constants in equation (26) are Planck’s constant, $h = 6.63 \times 10^{-34}$, the speed of light, $c = 2.99 \times 10^8 m/s$, the gap distance of the Fabry-Perot etalon, $d = 1.995 \times 10^{-3} m$, and the magnitude of the magnetic field at 10A, $B = 1.105 T$.

The calculated values for the Bohr magneton for each interference ring as well as the mean and standard deviation are given in Table 4.

Our calculated best value for the magnitude of the Bohr magneton is thus

$$\mu_B = 9.22 \times 10^{-24} \pm 0.06 \times 10^{-24} J \cdot T^{-1} \quad (27)$$

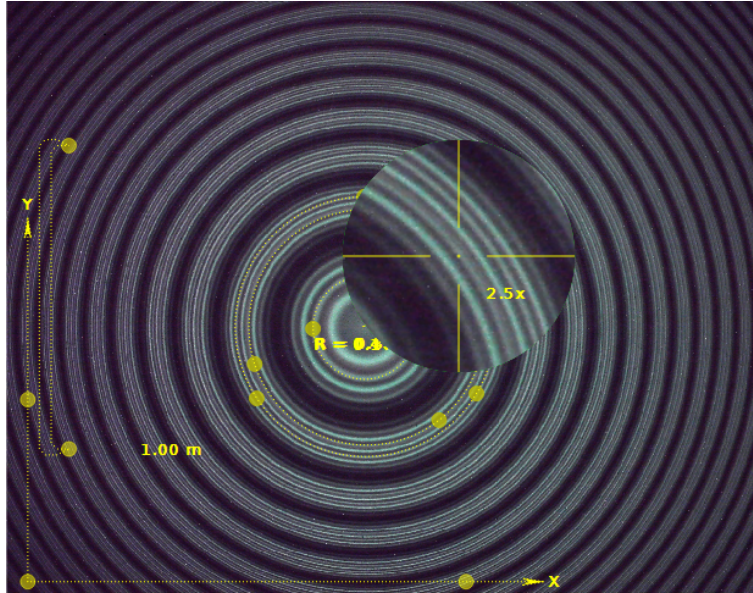


Figure 10: Mercury spectra in the presence of a magnetic field viewed without a polarizer. All spectra from all nine possible ΔM_z transitions can be seen.

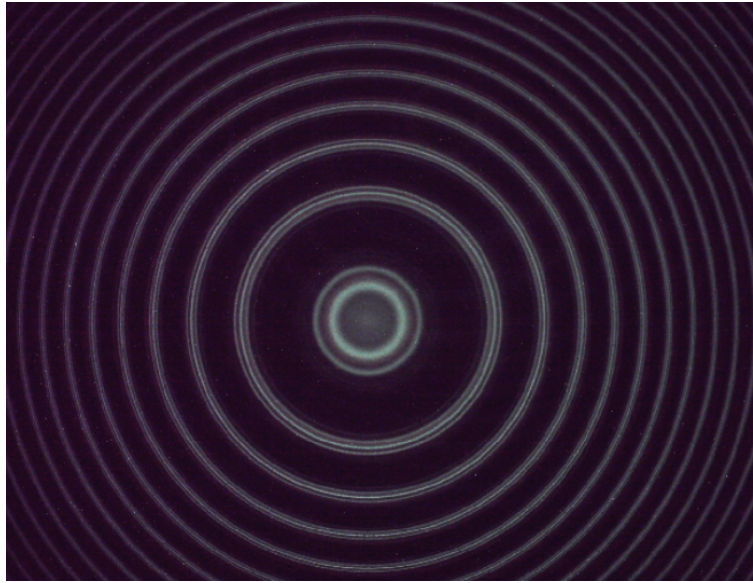


Figure 11: The ‘Normal’ Zeeman effect. Mercury interference pattern viewed perpendicular to the magnetic field lines through a polarizer oriented parallel to the field. The interference rings correspond to photons produced by $\Delta M_z = 0$ transitions polarized parallel to the magnetic field lines.

$k = 1$ Measurements	R_+ (m)	R_- (m)	ΔR (m)
1	0.4282	0.3893	0.0389
2	0.4278	0.3896	0.0382
3	0.4275	0.3887	0.0388
Mean	$0.4278 \pm 0.4 \times 10^{-3}$	$0.3892 \pm 0.5 \times 10^{-3}$	$0.039 \pm 0.4 \times 10^{-3}$
$k = 2$ Measurements	R_+ (m)	R_- (m)	ΔR (m)
1	0.5819	0.5539	0.0280
2	0.5815	0.5536	0.0279
3	0.5818	0.5536	0.0282
Mean	$0.5817 \pm 0.2 \times 10^{-3}$	$0.5537 \pm 0.2 \times 10^{-3}$	$0.0280 \pm 0.2 \times 10^{-3}$
$k = 3$ Measurements	R_+ (m)	R_- (m)	ΔR (m)
1	0.7035	0.679	0.0245
2	0.7033	0.6798	0.0235
3	0.7025	0.6805	0.0220
Mean	$0.7031 \pm 0.5 \times 10^{-3}$	$0.6798 \pm 0.8 \times 10^{-3}$	0.0233 ± 0.001
$k = 4$ Measurements	R_+ (m)	R_- (m)	ΔR (m)
1	0.8058	0.7861	0.02
2	0.8057	0.7865	0.02
3	0.8059	0.7857	0.02
Mean	$0.8058 \pm 0.1 \times 10^{-3}$	$0.7861 \pm 0.4 \times 10^{-3}$	0.020 ± 0.001

Table 2: Radius measurements of the hyperfine structure of the $k=1$ through $k=4$ interference rings with a 1T magnetic field and 90° polarization.

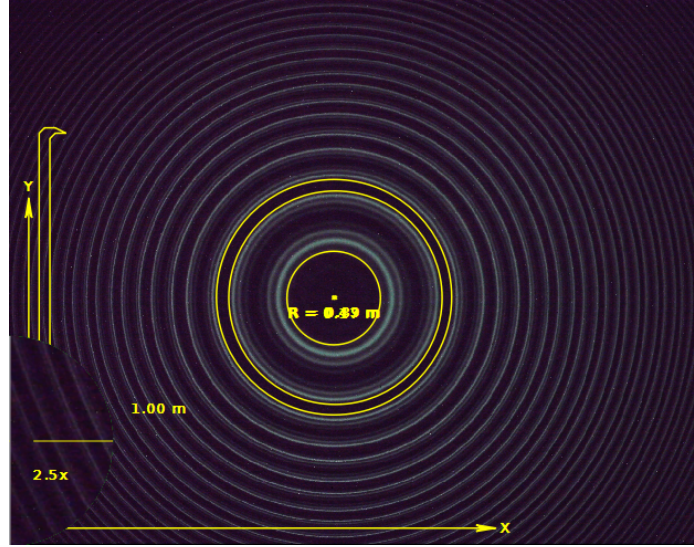


Figure 12: Interference pattern viewed through a polarizer oriented perpendicular to the magnetic field lines. The $\Delta M_z = 0$ transition spectra polarized parallel to the magnetic field cannot be seen, leaving a large gap between the circularly-polarized $\Delta M_z = \pm 1$ transition spectra.

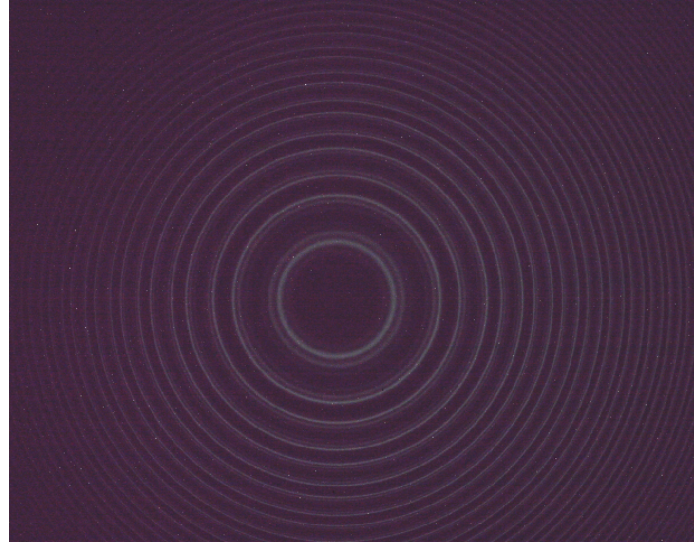


Figure 13: Interference pattern viewed axially along the magnetic field through the sight-hole in the electromagnet as shown in Figure 8b. Only the circularly-polarized $\Delta M_z = \pm 1$ transition spectra can be seen since photons from the $\Delta M_z = 0$ transition spectra cannot propagate in this direction because their **E** and **B** field vectors must be perpendicular to their propagation direction.

k	$C_0 \text{ (m}^{-2}\text{)}$
4	6.4523
3	6.4575
2	6.4633
1	6.4598
Mean	6.458 ± 0.005

Table 3: Measured values of the constant C_0 from the $B = 0$ interference rings.

k	$\mu_B \text{ (J} \cdot \text{T}^{-1}\text{)}$
1	9.16×10^{-24}
2	9.24×10^{-24}
3	9.36×10^{-24}
4	9.10×10^{-24}
Mean	$9.22 \times 10^{-24} \pm 0.06 \times 10^{-24}$

Table 4: Calculated values of the Bohr magneton μ_B for each interference ring, and the mean calculated value for all interference rings.

For comparison, the SI value of the Bohr magneton is $9.274 \times 10^{-24} \text{ J} \cdot \text{T}^{-1}$ [1], which is within our margin of measured random error. Additionally, our measured value agrees with the accepted SI value to within 0.63%.

4 Conclusion

We observed the Zeeman effect and verified its effect on the 546.1 nm mercury spectral line in the presence of a $\approx 1T$ magnetic field. We verified that the hyperfine structure was produced by transitions of various changes of the quantum number ΔM_z which are constrained by the quantum selection rules. Using a polarizer, we showed that the different hyperfine spectra have either parallel or circular polarization along the magnetic field lines. We were able to separately observe light polarized parallel to the magnetic field lines created in $\Delta M_z = 0$ transitions, as well as axially circular-polarized light created in $\Delta M_z = \pm 1$ transitions. Finally, we arrived at a measured value for the Bohr magneton of $\mu_B = 9.22 \times 10^{-24} \pm 0.06 \times 10^{-24} \text{ J} \cdot \text{T}^{-1}$, which is within 0.63% of the accepted SI value.

References

- [1] CODATA Value: Bohr magneton.
- [2] A.C. Melissinos. *Experiments in Modern Physics*. Academic Press, 1966.
- [3] Stigmatella aurantiaca. File:Etalon-2.svg, July 2012. Page Version ID: 502562557.